INTRODUCTION TO

the Solar Wind

JOHN C. BRANDT
NASA-Goddard Space Flight Center
Greenbelt, Maryland

That something besides light comes to the earth from the sun has long been suspected, but only in 1962, when Mariner II made direct measurements in space, was it established beyond doubt that a steady flow of ionized hydrogen particles sweeps out through the solar system. Since that time the solar wind has attracted the attention of increasing numbers of theorists and has been the object of many sophisticated space experiments, including one performed by the first men on the moon.

Introduction to the Solar Wind is the first systematic introduction to the subject. Written at an intermediate level, it covers all aspects from the stellar structure required to produce an extended atmospheric envelope, or corona, to the impact of the solar wind on the bodies of the solar system and the influence of stellar winds on stellar structure and evolution. All methods of observation are presented, although emphasis is on broad principles, which are treated as an integral and natural part of solar physics and astronomy.

The solar wind is important in discussions of topics as widely separated as the formation of ionic comet tails and the theory of general relativity and is therefore a remarkably unifying subject. Because *Introduction to the Solar Wind* treats all of the implications of the phenomenon in detail, it will be useful in a wide variety of courses for upper-division undergraduate and first-year graduate students. Such courses include those on the solar wind, the solar system, solar-terrestrial physics, solar physics, and others in departments of astronomy, physics, and electrical and aerospace engineering. *Introduction to the Solar Wind* is also an excellent introduction to the subject for scientists in other fields and for technical and professional workers in space-related research and engineering.

JOHN C. BRANDT is Chief of the Laboratory for Solar Physics at the NASA–Goddard Space Flight Center in Greenbelt, Maryland, and is Part-time Professor of Astronomy at the University of Maryland. He has been active in the study of the solar wind almost from the time an expanding solar corona was first theorized. He attended one of the first colloquia on the solar wind, conducted by E. N. Parker in 1959, and in the intervening years he has published more than two dozen papers on the solar wind and on directly related topics. The material that appears in *Introduction to the Solar Wind* was first developed for courses Professor Brandt taught at the University of Maryland.

Professor Brandt is a graduate of Washington University in St. Louis and received a Ph.D. in 1960 from the University of Chicago. In 1960-61 he was a Research Associate and a National Science Foundation Fellow at the Mount Wilson and Palomar Observatories. From 1961 to 1963 he was an Assistant Professor of Astronomy at the University of California, Berkeley. Before joining the NASA–Goddard Space Flight Center in 1966, Professor Brandt was Associate Astronomer in the Space Division of the Kitt Peak National Observatory in Tucson. He is the author of *The Sun and Stars,* coauthor with P. W. Hodge of *Solar System Astrophysics,* and coeditor with M. B. McElroy of *The Atmospheres of Venus and Mars.*

COVER: Photograph of the solar corona from the 1966 expedition of the High Altitude Observatory, National Center for Atmospheric Research. (Courtesy G. Newkirk, Jr.)

W. H. FREEMAN AND COMPANY
660 Market Street, San Francisco, California 94104
Warner House, Folkestone, Kent, England

A Series of Books in Astronomy and Astrophysics

EDITORS: Geoffrey Burbidge
Margaret Burbidge

INTRODUCTION TO

the Solar Wind

1970

John C. Brandt

NASA-Goddard Space Flight Center
Greenbelt, Maryland

Born 8-Aug-1934
PhD U. Chicago 1960

W. H. Freeman and Company
San Francisco

Contents

mass of the particle. If equation (1.2) holds, equation (1.1) integrates to

$$N(h_c) = (4\pi a^2 H)^{-1} \tag{1.4}$$

Physically, equation (1.4) places the critical level where the scale height equals the horizontal mean free path. Coronal densities and a mean collision cross section for protons place the critical level for solar mass loss at $2R_\odot$. The maxwellian velocity distribution is given by

$$f(v)\,dv = 4\pi(m/2\pi kT)^{3/2} v^2 e^{-(mv^2/2kT)}\,dv \tag{1.5}$$

The temperature of the corona is near 2×10^6 °K (see Section 2.4). The escape velocity differs from the usually quoted gravitational value because any tendency toward charge separation sets up an electric field. Let

$$\beta = \frac{eE}{m_p g_\odot} \tag{1.6}$$

be the ratio of electric to gravitational force on a proton. Then the equation of hydrostatic equilibrium can be written separately for protons and electrons as

$$m_p g_\odot - eE = (1-\beta) m_p g_\odot = kT_p \frac{d(\log_e N_p)}{dh} \tag{1.7}$$

and

$$m_e g_\odot + eE \approx \beta m_p g_\odot = kT_e \frac{d(\log_e N_e)}{dh} \tag{1.8}$$

The atmosphere is assumed to be isothermal, and the small mass of the electron allows the approximate equality in equation (1.8). There are enough collisions to keep the electron and proton temperatures nearly equal; similarly, an appreciable charge separation cannot occur (because of the strong restoring effects of the electric field that would result), and the proton and electron densities must be nearly equal. Thus, the right-hand sides of equations (1.7) and (1.8) are equal, and this fact implies $\beta \approx 1/2$. Thus, the electric field produces an "effective" proton mass of $m_p/2$, and the escape velocity for protons in a proton-electron mixture becomes

$$v_{esc}(\text{ion}) = \left(\frac{GM_\odot}{r}\right)^{1/2} \tag{1.9}$$

This result is a factor of $2^{1/2}$ lower than the neutral particle value. The situation is complex for other mixtures. The escape velocity for a proton at 2×10^6 °K from the solar surface is 435 km/sec while the corresponding

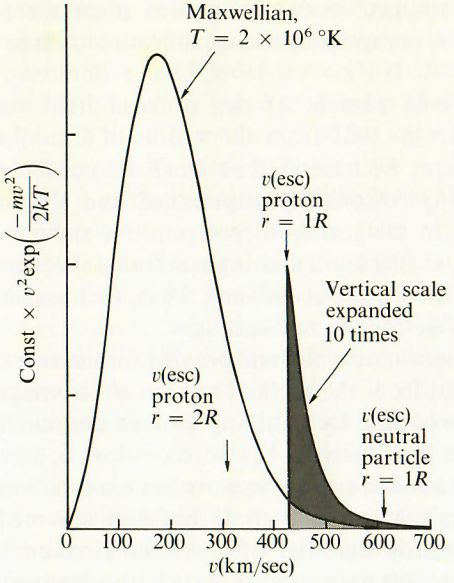

FIGURE 1.5
The maxwellian velocity distribution for $T = 2 \times 10^6$ °K showing various escape velocities.

neutral particle value is 616 km/sec. Appropriate values are shown in Figure 1.5, together with the maxwellian distribution for 2×10^6 °K. The particles available for escape are shown in the shaded area. Treatments differ as to the method of replenishing the escaping particles.

Contributions were made by Pikelner and Kiepenheuer, the subject of the coronal mass balance was reviewed by van de Hulst in 1953, and the evaporative-exospheric theory was extended by Chamberlain in 1960. While none of these early evaporative theories proved adequate, it is now possible to construct an exosphere model of the solar wind (Section 3.6). The error of the earlier treatments was in the use of a mean collision cross section in a plasma.

Evidence possibly pertaining to interplanetary gas was also available from study of the zodiacal light and whistlers. As noted above, for some years the zodiacal light had been attributed to the scattering or reflecting of sunlight by interplanetary dust. However, in 1953 Behr and Siedentopf published results concerning the degree of polarization and the brightness of polarized light in the zodiacal light. They found that the polarization was too high to be explained by dust scattering. (Not everyone agreed with their conclusion e.g., Fessenkov.) Hence, Behr and Siedentopf considered the possibility of scattering by interplanetary electrons. They calculated that an electron density near

corona can be preserved perpendicular to the lines of force because diffusion in this direction is greatly inhibited by the field. No such restriction exists along the lines of force; as a result, the long narrow features that were observed were expected. If the atmosphere is in hydrostatic equilibrium (or a close approximation thereto), the density gradients should be the same both in and out of the rays. This is the case because the pressure gradient is balanced by the gradient of the potential, and no magnetic term appears in the potential. The behavior of equal density gradients is predictable and apparently observed.

The density in a polar plume is about four to five times that of the immediate surroundings. This figure was reached after an analysis of tracings of polar regions on eclipse plates. For the 1900 eclipse, van de Hulst noted that single rays increased the coronal brightness by 10 percent and that the rays were about 7,000 km in diameter. Van de Hulst determined an effective path length of the polar corona and found that an individual ray diameter constituted some one-fortieth of the total. Therefore, the density must be enhanced by a factor of about four to produce a 10 percent increase in brightness. Similar enhancements were deduced from studies conducted during other eclipses. Enhancements of the same general amount over the normal coronal densities are found for streamers and helmets.

Besides the radial, fine structure associated with density fluctuations, there are other structural details often distinguished by enhanced intensity in certain emission lines. First, there are the fans or helmets, as noted earlier, which dominate the gross form of the corona. These are associated with quiescent prominences (Section 2.5); immediately above the prominence is a very dark region which is succeeded by a bright coronal arch system. Kiepenheuer has described the overall appearance of this entity in cross section as resembling the Eiffel Tower. The tip of this structure usually extends one or two solar radii above the limb; the base is usually about one-half a solar radius in width.

Streamers are extensions of the corona over active solar regions. They can be distinguished out to many solar radii and are fairly structureless; their thickness (or cross section) remains fairly constant with increasing radial distance.

Coronal or sporadic condensations are found only over very active or flaring groups. Usually they are found at the top of the active or sunspot prominences and in white light appear with an extent of a few times 10^4 km. Their density exceeds that of the surrounding medium by one or two orders of magnitude. These condensations have lifetimes of hours, or, at most, days (because this is the length of maximum activity associated with a sunspot group (see Section 2.5). Coronal condensations generally show the coronal yellow line of Ca XV at 5,694 Å; this line generally indicates a very high temperature.

Coronal enhancements or permanent condensations have base dimensions

comparable to plages (Section 2.5) and in many respects appear to be an extension of the plage activity into the corona. Their density is higher than the background corona but lower than the condensations. The enhancements can last for several solar rotations. During the time of maximum activity associated with a spot group, the innermost dense part of the enhancement may be described as a condensation. The coronal enhancements are often called coronal green patches because they are bright in the coronal green line of Fe XIV at 5,303 Å.

The terminology in studies related to solar activity is often quite confusing even to active workers in the field. Sometimes, for example, the same word is used to refer to two entirely different phenomena.

The coronal light may be divided into three components:

1. The K corona. This is continuous radiation resulting from photospheric radiation that is Thomson-scattered by free electrons in the corona.
2. The F corona (or false corona or inner zodiacal light). This is photospheric radiation diffracted by interplanetary dust. This radiation is not physically connected with the corona but must be accurately determined in order to separate it from the desired K corona.
3. The E or L corona. This is the total light of the coronal emission lines (optical region), such as the coronal green and yellow lines previously mentioned.

The brightness of the various components and other pertinent information are shown in Figure 2.8. The corona is often divided into the inner corona ($r/R_\odot \leq 1.3$), the medium corona ($1.3 \leq r/R_\odot \leq 2.5$), and the outer corona ($r/R_\odot > 2.5$); the latter region merges into the solar wind at large distances.

Densities. Coronal electron densities are calculated from photometric determinations of the brightness of the K corona. Often such measurements are presented in the form of isophotes. The K corona is presumed to originate by Thomson-scattering of photospheric radiation with cross section $\sigma = 6.6 \times 10^{-25}$ cm^2. The standard treatment assumes an optically thin corona. Thus, the coronal intensity at a particular frequency is simply the integral of the source function per unit volume along the line of sight, viz.,

$$4\pi I_\nu = R_\odot \int_{-\infty}^{+\infty} g(y)\, dy \tag{2.8}$$

Here y is in units of solar radii. The geometry is shown in Figure 2.9.

In order to continue, one must make some assumptions concerning symmetry which allows for the determination of three dimensional structure

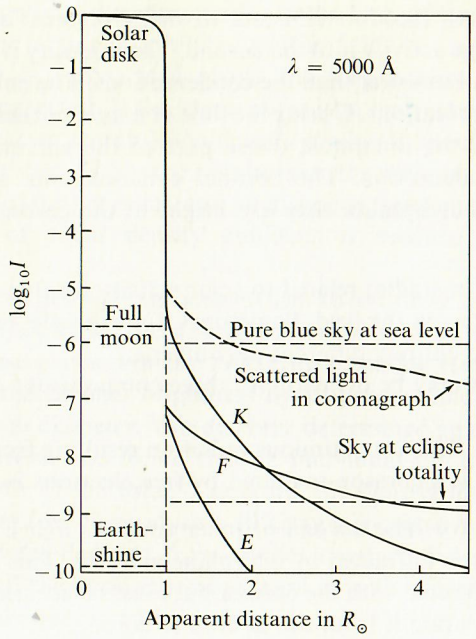

FIGURE 2.8
Schematic of the variation of the K, F, and E components of coronal light and other brightnesses of interest.

rom a two-dimensional light distribution. Spherical symmetry is often assumed and is adopted here. The assumption that Thomson-scattering is not isotropic involves very little error and is also used here. The source function per unit volume is then

$$g(r) = \sigma N_e(r) \int_{\text{solar disk}} \frac{I\, d\omega}{4\pi} \tag{2.9}$$

or

$$g(r) = \sigma N_e(r) J(r) \tag{2.10}$$

where $J(r)$ is the mean intensity of radiative transfer theory. It is determined by an integration of the emergent intensity over the solar disk taking account of limb-darkening; $J(r)$ varies approximately as $1/r^2$ and can be taken as known. Equation (2.8) can be written as

$$4\pi I_v = 2R_\odot \int_0^\infty [\sigma N_e(r) J(r)]\, dy \tag{2.11}$$

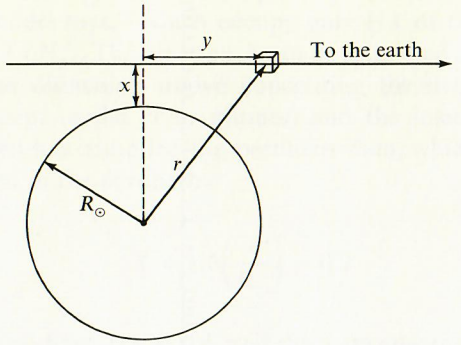

FIGURE 2.9
The geometry and nomenclature for computing the coronal electron density from observed brightnesses.

It is found by observation that the intensity of the K corona can be accurately expressed by a few terms of a sequence in inverse powers of r. Thus, one is led to consider a source function composed of inverse powers of r, or

$$g(r) = \sum_n a_n r^{-(n+1)} \tag{2.12}$$

The quantity r can be expressed in terms of y by considering the geometry as shown in Figure 2.9, and equation (2.11) can be rewritten for one term of equation (2.12) as

$$4\pi I_n = 2a_n R_\odot \int_0^\infty \frac{dy}{[(x + R_\odot)^2 + y^2]^{(n+1)/2}} \tag{2.13}$$

$$= \frac{2a_n R_\odot}{(x + R_\odot)^n} \int_0^{\pi/2} \cos^{n-1}\phi\, d\phi$$

Hence, an observed density component that varies as r^{-n} results from a source function component that varies as $r^{-(n+1)}$. If the intensity varies as a few terms of such a sequence, then it is a simple matter to determine the source function producing it; thus, $g(r)$ can be determined directly from observation. Note that there is no particular physical significance to these interpolation formulas.

If $g(r)$ is known, then $N_e(r)$ can be determined from equation (2.10) because $J(r)$ is known. Sample determinations of $N_e(r)$ are shown in Figure 2.10. The determination of the proton concentration requires the specification of the helium concentration; a hydrogen to helium ratio of 10:1 gives $N_p = 0.83\, N_e$.

The assumptions involved in the determination of coronal densities must also be kept in mind. The corona is assumed to be spherical and homogeneous,

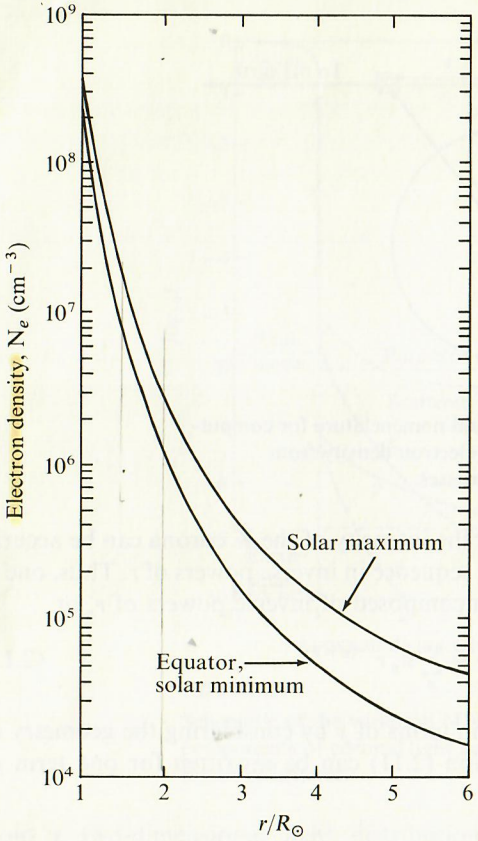

FIGURE 2.10
Some sample determinations of coronal electron density. (After C. W. Allen and H. van de Hulst.)

and the scattering is assumed to be isotropic. While all these assumptions produce some error, the assertion of homogeneity of the corona is probably the most serious. Some measure of the distribution of densities at a given r would be desirable; consider the function

$$\frac{1}{X} = \frac{\langle N_e \rangle^2}{\langle N_e^2 \rangle} \tag{2.14}$$

An entirely homogeneous corona has $1/X = 1$, and this function decreases for a corona with inhomogeneities. A simple interpretation follows from consideration of a sequence of n 1 cm^3 boxes, only one of which contains N_e electrons. The quantity $\langle N_e \rangle^2$ becomes $\langle N_e/n \rangle^2$ while $\langle N_e^2 \rangle$ becomes $\langle N_e^2/n \rangle$. Thus, $1/X = 1/n$ and leads to a simple interpretation of $1/X$ as the fraction of space occupied by matter. The densities determined from eclipse observations and the assumption of homogeneity are mean values, $\langle N_e \rangle$. A first step toward introducing the effects of the fine structure is to think of the mean density at a given r as determined by a combination of vacant regions

and so-called "model rays," which occupy only $1/X$ of the space but which have a density of $X\langle N_e \rangle$. The function X can be estimated from eclipse photographs (recall the discussion above concerning the determination of the density enhancement in the polar plumes) and the interpretation of radio observations. Allen has compiled the pertinent data, which may be approximately represented in the corona by

$$X = 1.6\left(\frac{r}{R_\odot}\right) - 0.7 \tag{2.15}$$

Thus, at $r = 2R_\odot$ we have $1/X = 0.4$, and this value decreases with increasing r. Such considerations are important in determining the coronal temperature from the gradient of electron densities.

Individual features, such as streamers, have been studied with the aid of an assumption concerning the depth of the feature—usually that the depth and breadth are comparable. A direct attack can be made on this problem by taking balloon observations with a sufficient time delay to allow the solar rotation to produce a stereoscopic effect. Reduction of such observations involves the assumption that the corona or feature under study is constant in time. The ultimate solution would involve simultaneous observations from a near-earth and a deep-space probe. This structural problem is very important because fans or streamers may mark the locations of the corona's prime contribution to the solar wind (see Section 7.1).

Temperature. The temperature of the corona is now well established as $\approx 10^6$ °K, but this is a relatively recent event. Prior to 1945, many exotic ideas were put forward to explain the existence of the coronal ions, which were ultimately identified by Grotrian and Edlén as highly ionized atoms of common constituents (e.g., Fe X). In 1945, Waldmeier summarized several different lines of argument, all of which required million-degree temperatures. It was from this time that a high-temperature corona was generally accepted. Billings has noted that "it is remarkable how many phenomena that had puzzled astronomers during the preceding century were explained by this concept."

There is much evidence now on the temperature of the corona. It can be determined from the variation of electron density with r and the assumption of hydrostatic equilibrium; the simplest case also assumes an isothermal corona. Such an atmosphere with spherical symmetry has a density distribution given by

$$\frac{N_e}{N_{e,0}} = \exp\left[\frac{GM_\odot m_H \mu}{R_\odot kT}\left(\frac{1}{r} - \frac{1}{r_0}\right)\right] \tag{2.16}$$

where G is the constant of gravitation, $M_\odot$ the mass of the sun, μ the mean molecular weight, m_H the mass of the hydrogen atom, $R_\odot$ the solar radius, k the Boltzmann constant, T the temperature, r the heliocentric distance in solar radii, and the subscript zero denotes a reference level. Equation (2.16) implies a linear variation between log N_e and $(1/r)$ with the slope determined by the temperature and the mean molecular weight. If we take logarithms of equation (2.16), differentiate, and solve for the temperature, we find

$$T = \frac{1.00 \times 10^7 \mu}{d \log_{10} N_e / d(1/r)} \tag{2.17}$$

For a composition of 10 hydrogen atoms to 1 helium atom, $\mu = 0.608$. Plots of log N_e versus $(1/r)$ for the equatorial region show a straight line behavior out to about $3R_\odot$ with a slope $d \log_{10} N_e/d(1/r) = 4.0$. This simple approach determines a temperature of 1.5×10^6 °K. Slightly lower temperatures are sometimes quoted for the polar corona, but they should be treated with caution because it is difficult to obtain data which unambiguously refer to the polar regions.

Equation (2.17) ignores any possible expansion of the corona (as implied by the solar wind) and the effects of fine structure. The equation of motion for a spherically symmetric expanding corona is

$$\frac{d\tau}{d\eta} + \tau \frac{d \ln \langle N_e \rangle}{d\eta} + \frac{\mu m_H}{kT_0}\left(R_\odot g_\odot \eta^{-2} + w \frac{dw}{d\eta}\right) = 0 \tag{2.18}$$

where $\tau = T/T_0$, T_0 the temperature at a reference level, $\eta = r/R_\odot$, w the expansion velocity, $g_\odot$ the acceleration of gravity at the solar surface, and $\langle N_e \rangle$ the average electron density as determined from eclipse studies. The observed electron densities can be fitted with a sequence of inverse powers of η and equation (2.18) solved for the temperature; the solution requires the specification of T_0 and the determination of $w\, dw/d\eta$. The solar wind flux and the constant in the equation of continuity, $N_e w r^2 = \text{const.}$, are assigned by quantities observed directly near the earth. The known densities and the equation of continuity determine the term $w\, dw/d\eta$. The integration constant T_0 is determined by the form of the equation and the unstable nature of the solutions; T_0 is very well determined simply by insisting that the temperature be neither negative nor infinite in the range 1.1 to $7R_\odot$. Sample results are shown in Figure 2.11.

The effects of the fine structure can be included by noting that part of the observed or apparent decrease in the coronal electron density is actually due to the steady decrease in the fraction of space occupied by matter, as shown in equation (2.15). Only the physical decrease in the "model rays" is relevant to the temperature determination, and the temperature is calculated by replacing $\langle N_e \rangle$ in equation (2.18) with $X\langle N_e \rangle$. These temperatures are also shown in Figure 2.11.

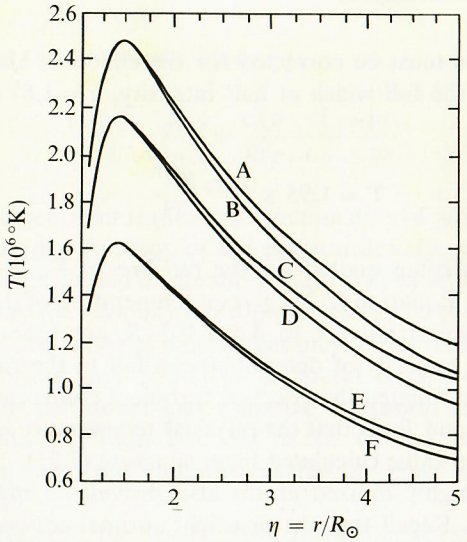

FIGURE 2.11

The temperature distribution as computed from electron densities under various assumptions including a flux ($N_e w$) at earth of 1×10^8 particles/cm^2-sec where applicable.
(A) Inhomogeneous expanding model, H:He = 5:1.
(B) Inhomogeneous static model, H:He = 5:1.
(C) Inhomogeneous expanding model, H:He = 10:1.
(D) Inhomogeneous static model, H:He = 10:1.
(E) Homogeneous expanding model, H:He = 10:1.
(F) Homogeneous static model, H:He = 10:1.
(After J. C. Brandt, R. W. Michie, and J. P. Cassinelli.)

The calculated temperatures for $r < 4R_\odot$ are not greatly changed by the expansion; they are, however, significantly changed by the inclusion of the fine structure. A coronal temperature of about 2×10^6 °K would follow from these curves. The values are entirely consistent with the other methods of determining T (as discussed below) except for the region just above the transition zone: the spectroscopic evidence for that region appears to require a much steeper gradient.

Spectroscopically, the temperature can be determined from measurements of the profiles of the coronal emission lines. If the line is broadened only by the Doppler effect and the corona is optically thin, the profile follows the law

$$\frac{I}{I_0} = \exp - \frac{(\lambda - \lambda_0)^2}{(\delta\lambda_0)^2} \tag{2.19}$$

where I is the intensity, λ is the wavelength, and the subscript zero refers to the line center. The Doppler width is given by

$$\delta\lambda_0 = \frac{\lambda}{c}\left(\frac{2kT}{\mu m_H}\right)^{1/2} \tag{2.20}$$

The raw observations must be corrected for the effects of the instrumental profile to determine the full width at half intensity, $h = 1.67\,\delta\lambda_0$. The temperature is then

$$T = 1.95 \times 10^{12}\,\frac{\mu h^2}{\lambda^2} \tag{2.21}$$

Observational results often quoted for the red line of Fe X ($\mu = 55.85$) at 6,375 Å are $h = 0.89$. Equation (2.21) gives a temperature of 2.1×10^6 °K. A variety of temperatures from 1.2 to 4.5×10^6 °K are found for different coronal regions; the majority of determinations fall in the range $2.0\text{–}2.5 \times 10^6$ °K. Billings has estimated the effect of turbulent control motions on the derived temperature and finds that the physical temperature is about 0.25×10^6 °K lower than the value calculated from equation (2.21).

The existence of highly ionized atoms also provides a means for determining temperatures. Recall that the principal coronal emission lines in the traditional wavelength region are the green line (5, 303 Å) of Fe XIV, the yellow line (5,694 Å) of Ca XV, and the red line (6,375 Å) of Fe X; the ionization potentials of these ions are 355, 820, and 235 ev, respectively. The simple observation of species with such high ionization potentials immediately suggests a very high temperature.

The circumstances that permit the direct observation of the optical coronal emission lines may be somewhat fortuitous. Ions expected for temperatures $\sim 10^6$ °K have large energy differences between the lower states, and transitions between them would fall in the extreme ultraviolet region of the spectrum. However, the ground terms of these ions are split into levels which have energy differences lying in the optical range. These levels are metastable, and the Einstein A's referring to transitions between them are $\sim 10^2 \mathrm{sec}^{-1}$; contrast this with Einstein A's $\sim 10^7 \mathrm{sec}^{-1}$ for typical permitted transitions. This fact requires a low density medium for the lines to be visible. A high density medium would de-excite the upper level by collisions during the relatively long time spent there. Fortunately, the coronal density is low enough to satisfy this condition.

The population of ions in the various stages of ionization as a function of temperature is determined by a balance of loss-and-gain processes for a given stage of ionization. The relevant processes in the corona are collisional ionization, and radiative and/or dielectronic recombination between adjacent stages of ionization and a balance is necessary for a steady state. Denote the stage of ionization by p, the collisional ionization coefficient by C, and the recombination coefficient by R. The balance between adjacent stages gives

$$N_e N_p R(p \to p-1) = N_e N_{p-1} C(p-1 \to p). \tag{2.22}$$

If there are N ions in the $(p-1)$ and p-th stages of ionization, then we can introduce the degree of ionization x such that there are $N(1-x)$ in the $(p-1)$ stage and Nx in the p-th stage. Then,

$$\frac{x}{1-x} = \frac{C(p-1 \to p)}{R(p \to p-1)} \tag{2.23}$$

Note that the degree of ionization is a function only of temperature and atomic parameters and not a function of the electron density.

If the coefficients needed in equation (2.23) are available, the distribution of a given element in the various ionization stages can be computed as a function of temperature. The ratios of ionic stages must be extracted from the observations of the optical lines and from a careful discussion of the excitation conditions. Both collisional and radiative excitation are important, and a detailed calculation is required; low in the corona ($\approx 1.1\,R_\odot$), collisional excitation dominates, but radiative excitation must still be included for numerical accuracy.

Until rather recently, the observations and available rate coefficients yielded temperatures close to 0.8×10^6 °K. However, in 1964 Burgess re-examined the calculations of the recombination coefficient and concluded that an alternate process, dielectronic recombination, was important and would change temperatures that were inferred from studies of line intensities. The older, radiative recombination coefficients were derived on the basis of the continuum electron's energy (kinetic energy + binding energy) upon recombination being given up in a photon of the same total energy. If, however, a continuum electron has an energy equal to the excitation energy of two bound states, it can excite a bound electron to one of these states and occupy the other. This yields a recombined atom with two excited electrons which cascade to lower states and emit radiation. Thus, two electrons are involved in this process, and, hence, the name, dielectronic recombination. In very hot plasmas, such as the corona, dielectronic recombination is more efficient than ordinary radiative recombination, and the recombination rate is increased by about one order of magnitude. To produce the same observed degree of ionization, the ionization rate (which increases with increasing temperature) must also increase. The analysis indicates a temperature of about 2×10^6 °K.

The ionic temperatures can be estimated directly with the aid of mass spectrometer determinations of the composition of the solar wind obtained by the Vela group (Section 5.4). Several different ionization stages of oxygen were observed, and it was easily established that the ionization balance was fixed in the corona at $r \approx 1.5\,R_\odot$. The temperature was found to be 1.7×10^6 °K, but this value may be representative of relatively cool solar wind plasma at the earth.

Sometimes ratios of lines from different elements or widely separated stages of ionization are used to infer a temperature or a change in temperature with heliocentric distance. The ratio of the green line (Fe XIV) to red line (Fe X) intensities is often used. Unfortunately, the ionization potentials of the two

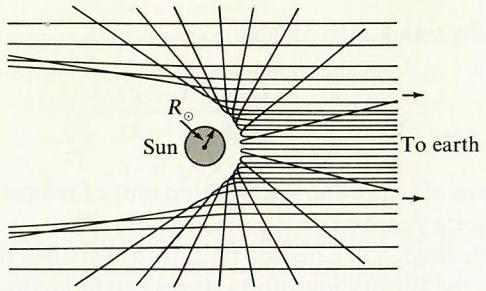

FIGURE 2.12
Ray paths in the corona at 18 Mc/s. (After R. N. Bracewell and G. W. Preston.)

onic species differ by 120 ev. Thus, possible coronal fine structure suggests caution; from observation, the fine structure seems clearly to be present because the widths of the red line consistently correspond to lower temperatures than do the widths of the green line. Apparently there are different temperature regions on a scale too fine to be resolved by present observational techniques. Information obtained from line ratios (such as the green line:red line) must be regarded as primarily qualitative.

Another indication of the coronal temperature is the widths of the Fraunhofer lines in the scattered K corona. The Fraunhofer lines are generally undetectable, with the possible exception of the H and K lines of Ca II. Equation (2.21) can be solved for the full width at half intensity h for $T = \times 10^6$ °K and for the atomic weight of the electron, $\mu = 1/1{,}836$. These numbers give $h \approx 170$ Å. The observations are very difficult, and present results are consistent with any temperature greater than about 10^5 °K.

The final "prime" method for determining the coronal temperature is the solar radio brightness temperature for frequencies of about 18 Mc/sec. Assuming a homogeneous corona and using Snell's law, one can calculate, the ray paths through the corona for a medium with a varying index of refraction. The index of refraction varies according to

$$n = \left[1 - \frac{e^2 N_e}{\pi m_e} \frac{1}{f^2}\right]^{1/2} \tag{2.24}$$

where e is the electronic charge, N_e is the electron density, m_e is the mass of the electron, and f is the frequency of the radio wave. The plasma frequency is defined by $f_0 = (e^2 N_e/\pi m_e)^{1/2}$.

The behavior of the ray paths in the corona is especially interesting. The ray which approaches closest to the sun is the one toward the center of the disk; this ray approaches to a distance such that $n = 0$ or $f = f_0$. Other rays from a given observing location do not penetrate farther into the solar atmosphere (see Figure 2.12). If one chooses to keep the wavelength close to

ten meters, the ray path can be confined entirely to the corona. If the assumption of a homogeneous corona is essentially correct, then radio observations of the corona can be carried out in the radio wavelength range without the contaminating "glare" of the photosphere. Thus, radio observations are a potentially valuable source of observations of the corona against the solar disk. Some complications are expected from the existence of the solar magnetic field, but these should be important only over large sunspots where a substantial magnetic field could be present.

The equation of transfer for radio wavelengths is derived with consideration of the change of intensity caused by the varying index of refraction. Thus, (I/n^2) is constant if there are no absorbing or emitting processes. The standard equation of transfer can be integrated to yield the emergent intensity, or

$$I = \int_0^{\tau_0} e^{-\tau} B(T)\, d\tau \tag{2.25}$$

The integration is carried out along the ray path which is computed as described above. The opacity is also given by a line integral

$$\tau = \int_s^{\infty} K\, ds \tag{2.26}$$

where K is the absorption coefficient.

The emission per unit frequency in the corona is given by the Planck function,

$$B_\nu(T) = \frac{2h\nu^3}{c^2} \frac{1}{e^{h\nu/kT} - I} \tag{2.27}$$

The Planck function is permissible in the corona because only a maxwellian velocity distribution is required, not an approach to local thermodynamic equilibrium. The physical interpretation of equation (2.25) gives the emergent intensity as the emission from each point along the trajectory reduced by the intervening opacity.

In the radio wavelength range, the Planck function can be replaced by the Rayleigh-Jeans approximation, $B(T) = 2kT/\lambda^2$. Similarly, the intensity in the radio region is related to the brightness temperature T_b through $I = 2kT_b/\lambda^2$. Hence, equation (2.25) can be written as

$$T_b = \int_0^{\tau_0} T e^{-\tau}\, d\tau \tag{2.28}$$

If the temperature T_c is constant in the corona, then

$$T_b = T_c(1 - e^{-\tau_0}) \tag{2.29}$$

The observations would appear to determine the coronal temperature, and values close to 1×10^6 °K are cited in the literature. However, the situation is

complex, especially for the optically thin case. The optical depth for thermal emission (free-free transitions) is proportional to $N_e^2/T^{3/2}$, and, hence, the emission is proportional to $N_e^2/T^{1/2}$. Thus, the problem of the coronal radio temperature is closely coupled with the problem of determining the opacity along the ray path. Most radio workers quote coronal temperatures of about 1×10^6 °K (for an optically thick corona), although considerable uncertainty exists. If such temperatures are correct, a bona fide discrepancy exists between them and coronal temperatures that have been inferred by other means. This possible discrepancy has led to a questioning of the basic equation of transfer. The problem has been hotly discussed, but the present consensus is in support of the traditional equation of transfer and holds that it is not the source of the discrepancy. Perhaps, the cause is inherent in the analysis or the result of coronal irregularities. Very recent results with greatly improved resolution give higher temperatures in essential agreement with other methods.

Finally, the temperatures can be inferred from the decay times of Type III radio bursts on meter wavelengths. The Type III bursts appear to be plasma oscillations at the plasma frequency excited by a fast group of particles (electrons) traveling through the solar atmosphere at speeds of about $c/3$ to $c/2$. The plasma frequency can be computed as a function of height in the corona from an assumed model, and thus the frequency drift with time gives the velocity of the exciting disturbance. Plasma oscillations will damp out due to collisions between ions and electrons, as $e^{-\nu t}$ where ν is the collision frequency in the plasma; the collision frequency is proportional to $N_e/T^{3/2}$. The density can be obtained because the oscillation is at the local plasma frequency [see equation (2.24)]. Hence, measurement of ν determines the temperature. Values of T near 2.5×10^6 °K are generally quoted although there are uncertainties and exceptions. The value that was quoted is entirely compatible with the temperature expected for the corona over an active solar region.

In summary, most available evidence indicates a coronal temperature near 2×10^6 °K. No serious conflict exists at the present time.

Composition. The composition of the corona influences many other coronal investigations and is an interesting topic in itself. The temperature inferred from density gradients [equations (2.17) and (2.18)] is directly proportional to the mean molecular weight in the corona, which is determined entirely by the relative abundance of helium in the corona. Exactly the same observed gradient gives a 22 percent higher T for H:He = 10:1 ($\mu = 0.608$) than for a pure hydrogen corona ($\mu = 0.5$). Commonly accepted values of H:He are near 10:1, and the temperature thus derived is compatible with values obtained by other means. However, the coronal helium abundance cannot be determined directly because helium is completely ionized in the corona.

An indirect determination can be attempted by fitting the relative abundance of He in solar cosmic rays onto the photospheric (spectroscopic) abundances

of the other elements. A detailed analysis gives the ratios of C, N, and O to H for the photosphere; a specific result is log [N(O)/N(H)] = −3.23. Cosmic ray results for He, C, N, and O are available. The charge to mass ratios of these nuclei are the same, and their relative abundance should remain constant through the flare process. Their relative abundances are reasonably constant from event to event, and the relative abundances of the C, N, and O nuclei are in reasonable agreement with the spectroscopic results. The cosmic ray ratio is N(He)/N(O) = 107, and the combination gives N(He)/N(H) = 0.06. This number is some sort of average between the photosphere and the flare location. The coronal density of helium could be higher (see Section 5.4).

An abundance of heavier elements, such as iron, can be determined from analyses of the optical lines from the ion. The absolute line intensity gives the total number of ions in the appropriate upper level along the line of sight, and a detailed calculation is involved in determining the total iron abundance. The uncertainties in such a calculation cannot be minimized, but for more than two decades many calculations have indicated an overabundance of the heavy elements relative to the photospheric abundances. Typical values show that iron is some ten to twenty times more abundant (relative to hydrogen in the corona as compared with the photosphere). This result could involve a process of diffusion or a mass dependent solar wind. This subject is discussed further in Section 5.4.

The Magnetic Field. A general magnetic field in the corona can be inferred from the results of a variety of indirect methods. Recall the previous discussion of coronal fine structure and the polar plumes. The field is apparently required for support of prominences, channeling of moving prominence material, and the form of coronal material around solar-active regions. The magnetic field is assumed in many calculations concerning the theory of the corona, such as the problem of mechanical heating. The indirect evidence and the attempts to measure the coronal magnetic field have been reviewed by Billings.

Despite the prima facie nature of considerable traditional evidence, the best evidence comes from space probe measurements of B near the earth. This near-earth field is apparently the photospheric field which is convected by the solar wind. This fact is established by evidence of a close correlation between the solar and interplanetary field with a time delay of about five days (Section 5.6). The quiet-time interplanetary measurement gives a radial field $B_r = 3.5\gamma(1\gamma = 10^{-5}$ gauss). An inverse square variation of this component with distance implies a surface field of 1.5 gauss, a value in excellent agreement with the surface measurements. Thus, an inverse square law with a surface field of 1.5 gauss gives a good *typical* value for the field in the corona. Much higher fields can be expected in the corona over centers of solar activity. (see Section 7.1 for discussion of the possible configurations of the field in the corona.)

$1\gamma = 10^{-5}\,G = 10^{-9}$ Tesla

3

Basic Theory

This chapter covers the development of the theoretical approach to the solar wind, beginning with the original hydrodynamical model of E. N. Parker. The evolution of theoretical models is traced, with some attention being paid to the inclusion of the magnetic field. Finally, the extent of the solar wind into space is discussed in terms of its interaction with the interstellar medium.

3.1 Parker's Hydrodynamic Theory (1958)

Parker began his paper by developing two points: (1) there was considerable evidence from studies of comet tails and from geomagnetic studies that favored a continuous expulsion of solar matter at speeds of hundreds of km/sec, and (2) Chapman's static model had a much larger pressure at infinity than could be balanced by the pressure of the interstellar medium; hence, it was postulated the interplanetary medium must expand. (This point has been discussed in Section 1.3.)

Parker proposed that the expansion was a natural result of the high temperature of the corona, and to illustrate this he worked out the first

hydrodynamic model, based on a scalar pressure. The corona is assumed to be spherically symmetric, inviscid, and in a steady state; the sun is assumed to be nonrotating and to have no magnetic field. The basic hydrodynamic equations are: (1) the equation of motion

$$N\mu m_H w \frac{dw}{dr} = -\frac{d}{dr}(NkT) - \frac{GN\mu m_H M_\odot}{r^2} \tag{3.1}$$

and (2) the equation of continuity

$$N(r)w(r)r^2 = N_0 w_0 a^2 = C \tag{3.2}$$

Here,

N = the total particle density,
m_H = the mass of the hydrogen atom (1.67×10^{-24}g),
μ = the mean molecular weight,
w = the radial expansion velocity,
r = the heliocentric distance,
k = Boltzmann's constant (1.4×10^{-16}erg/°K),
T = the temperature,
G = the gravitational constant (6.67×10^{-8} cm^3/g-sec^2),
$M_\odot$ = the mass of the sun (1.99×10^{33}g).

The notation introduced by Parker was

$$\xi = r/a \tag{3.3}$$

$$\tau = T(r)/T_0 \tag{3.4}$$

$$\lambda = \frac{G\mu m_H M_\odot}{akT_0} = \frac{(V_{esc})^2}{U^2} \tag{3.5}$$

$$\psi = \frac{\mu m_H w^2}{kT_0} = \frac{w^2}{U^2} \tag{3.6}$$

In all of the above equations, the subscript zero refers to the quantity evaluated at the base of the corona $r = a$; and $U = (2kT_0/m_H)^{1/2}$ is the most probable velocity of protons in a maxwellian distribution at temperature T_0. The density can be eliminated from equation (3.1) using equation (3.2) and the resulting equation written in terms of the variables defined by equations (3.3) through (3.6). This gives

$$\frac{d\psi}{d\xi}\left(1 - \frac{\tau}{\psi}\right) = -2\xi^2 \frac{d}{d\xi}\left(\frac{\tau}{\xi^2}\right) - \frac{2\lambda}{\xi^2} \tag{3.7}$$

Although the detailed nature of the solution requires the specification of $T(r)$, the basic form is evident from inspection of equation (3.7). Equation (3.8) shows that the right-hand side of equation (3.7) has a zero. The left-hand side can become zero either by having $d\psi/d\xi = 0$ or by having $\tau = \psi$. This feature suggests a dual nature of the solutions. Low in the corona, $d\psi/d\xi$ is positive as the plasma accelerates. Hence, if the equation is satisfied by $d\psi/d\xi = 0$, the velocity will decrease thereafter. If the equation is satisfied by $\tau = \psi$ and not $d\psi/d\xi = 0$, then ψ will increase outward.

Parker set $\tau = 1$ (constant temperature) to approximate the conditions appropriate to the high thermal conductivity of the corona. If thermal conduction alone was insufficient to maintain a constant temperature, energy deposition could be invoked. Then, with the r.h.s. of equation (3.7) equal to zero or

$$2\xi^2 \frac{d}{d\xi}\left(\frac{1}{\xi^2}\right) + \frac{2\lambda}{\xi^2} = 0 \tag{3.8}$$

this reduces to

$$\frac{\lambda}{\xi^2} = \frac{2}{\xi} \tag{3.9}$$

Since the l.h.s. of equation (3.9) is larger than the r.h.s. low in the corona and also decreases faster with increasing distance, the two sides can be equal to produce a zero in the r.h.s. of equation (3.7). This occurs at

$$\xi = \frac{\lambda}{2} = \frac{G\mu m_H M_\odot}{2akT_0} \tag{3.10}$$

Parker chose the solution for which $\tau = \psi$. This latter condition implies $\mu m_H w^2 = kT$, and, hence, the thermal and bulk kinetic energies are approximately equal at the point defined by equation (3.10), which is called "the critical point." The velocity at this point is

$$w = \left(\frac{kT}{\mu m_H}\right)^{1/2} \tag{3.11}$$

Since this is close to the velocity of sound,

$$v_s = \left(\frac{\gamma P}{\rho}\right)^{1/2} = \left(\frac{5kT}{3\mu m_H}\right)^{1/2} \tag{3.12}$$

the critical point is sometimes loosely referred to as the "sonic point" and the solutions advocated by Parker as the "supersonic solutions." Choice of the solutions for which $d\psi/d\xi = 0$ at the critical point would limit the expansion

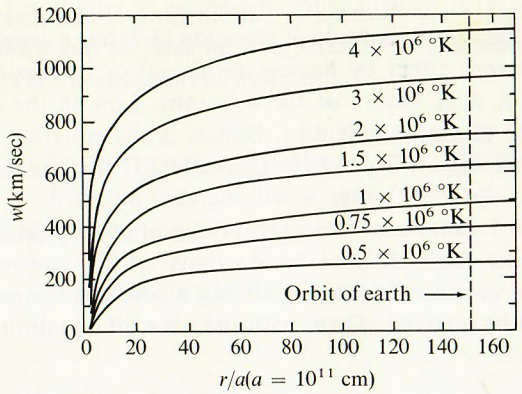

FIGURE 3.1
Parker's solar wind solutions (isothermal corona) based on Equation (3.13). (After E. N. Parker.)

velocities to less than the value given by equation (3.11) or 180 km/sec for $T = 2 \times 10^6$ °K. Such velocities could not reproduce Biermann's observations.

The solution of equation (3.7) for the isothermal case such that $\psi = 1$ at $\xi = \lambda/2$ is given by

$$\psi - \ln \psi = -3 - 4 \ln \frac{\lambda}{2} + 4 \ln \xi + \frac{2\lambda}{\xi} \tag{3.13}$$

As one moves away from the sun, the dominant terms are

$$\psi \approx 4 \ln \xi \tag{3.14}$$

and, hence, the isothermal region must be terminated at some finite distance. Figure 3.1 shows solutions calculated from equation (3.13). If we seek solutions which reach a velocity of 500 km/sec, this velocity is reached at $r = 5a$ for $T_0 = 3 \times 10^6$ °K, $r = 16a$ for $T_0 = 2 \times 10^6$ °K, and $r = 36a$ for $T_0 = 1.5 \times 10^6$ °K. A cutoff distance of some 20a would be quite reasonable. Note that some simplifications were introduced in the original calculations, such as setting the solar radius $= a = 10^{11}$cm.

Thus, Parker showed that velocities $\sim 10^3$ km/sec could result from coronal temperatures existing over an extended region around the sun. The outflowing gas suggested by Biermann was then explainable in terms of the high temperature of the corona. The density at the earth's orbit was approximately 500 electrons/cm^3 on the early models; this value is now known to be too high by a factor of about 10^2. The discrepancy results apparently from the assumed temperature distribution and/or filamentary structure in the corona.

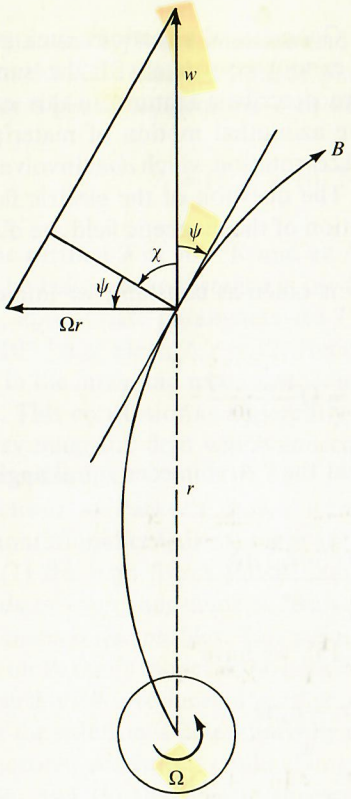

FIGURE 3.2
Schematic of the spiral form of the interplanetary magnetic field and the quantities used to describe it.

Note that the supersonic solutions obtained by Parker cannot occur if the coronal temperature is too high. This can be seen by solving for T_0 in equation (3.10) for $\xi = 1$ to obtain $T_0 = 4 \times 10^6$ °K. A higher T_0 would displace the critical point below the solar surface. The physical reason for this limit is discussed in Section 3.3.

Parker also discussed the form of the magnetic field if it is carried into space by steady expansion but with the roots of the field lines fixed on a rotating sun. Assume that the solar wind plasma cannot cross the magnetic field lines, i.e., that the field lines are frozen-in. The interplanetary field lines then connect all plasma emitted from the same location on the rotating sun and have an "Archimedes" spiral configuration as shown in Figure 3.2.

The spiral field pattern rotates with the solar (twenty-seven-day) period while the plasma moves strictly radially. This apparent contradiction can be visualized by imagining the grooves of a phonograph record and the needle (as suggested by Ahluwalia and Dessler). Just as the grooves determine the path of the needle, so does the plasma determine the shape of the field. The condition for co-rotation on this picture follows from quantities defined in

igure 3.2 and is $w \sin \psi = \Omega r \cos \psi$. Geometrical situations such as kinks flare-induced changes in the field cannot co-rotate with the sun. Note at the concept of co-rotation used to describe a feature, in this case, the agnetic field, which does *not* involve azimuthal motion of material must e carefully distinguished from physical co-rotation which *does* involve azimuthal motion of material (Section 3.7). The question of the electric field and her problems associated with co-rotation of the magnetic field are discussed Section 3.7.

If Ω is the solar rotation rate and w is taken as constant, we immediately ave

$$\phi - \phi_0 = \Omega t = \Omega \frac{(r_0 - r)}{w} \tag{3.15}$$

eferring to Figure 3.2 again, we see that the "Archimedes spiral angle" ψ is defined by

$$\tan \psi = -\frac{(r - r_0)\, d\phi}{dr} \tag{3.16}$$

nce $-d\phi/dr = \Omega/w$ from equation (3.15), we have

$$\tan \psi = \frac{(r - r_0)\Omega}{w} \tag{3.17}$$

e quantity $r\Omega$ is the linear velocity that corresponds to rigid body solar tation at the earth and is approximately 430 km/sec. Thus, if $w \approx 430$ n/sec, the interplanetary magnetic field lines near the earth should make an gle of 45°, or 135° with the radius vector. Such behavior has been observed, d is discussed in Section 5.5.

In the preceding discussion we assumed that the field lines were frozen-in the plasma. This can be calculated from the magnetic Reynolds number

$$R_M = [4\pi\sigma\, l^2]/[l/w] = 4\pi\sigma\, lw \tag{3.18}$$

ere l is a characteristic dimension and the conductivity $\sigma = 2 \times 10^{-14}$ ^{2} (c.g.s. units). Physically, the magnetic Reynolds number is the ratio of the e required for a magnetic field to diffuse through a distance $l(\tau_{\text{dif}} = 4\pi\sigma\, l^2)$ the time required for the field to be transported through a distance l by lk motions ($\tau_{\text{trans}} = l/w$). If the Reynolds number is very large, the field is zen-in. For $w = 5 \times 10^7$ cm/sec, $\sigma \approx 10^{-6}$ (for $T \sim 10^5$ °K), and $l = 10^{13}$, we obtain $R_M \sim 10^{16}$ and the field is certainly frozen-in.

Lastly, the assumption of a scalar pressure [implicit in the form of equation 1)] required justification. Certainly the mean free path for protons should

be less than the typical dimension and can be calculated in a proton-electron gas from the 90° deflection time of plasma physics (t_D) and the mean proton speed for a gas at temperature T to obtain

$$\Lambda = (1/2) \times 10^{-9} \frac{T^2}{N_e} \qquad \text{(a.u.)} \tag{3.19}$$

Near the earth, a T of 10^5 °K and an N_e of 5/cm^3 are appropriate and $\Lambda = 1$ a.u. If the heliocentric distance is used as the typical dimension, $\Lambda/r = 1$. At 2.5 $R_\odot$, appropriate parameters are $T = 1.5 \times 10^6$ °K and $N_e = 10^6$/cm^3 for a Λ of 10^{-3} a.u. Here, $\Lambda/r = 12$. Hence, a scalar pressure is a good approximation in the inner and medium corona, but not for the distant reaches of the corona. This conclusion is apparently modified by the presence of the interplanetary magnetic field which can couple particles together and effectively provide collisions.

Objections to Parker's theory were immediate and widespread. Besides many nonrational criticisms, three substantial points against the theory were made: (1) the high fluxes found from the model implied flow velocities of hundreds or even thousands of km/sec in the corona, and effects should be seen in coronal line profiles. This point is well taken, and it is now known that the flux on Parker's model is too high by a factor of 10^2. A less severe temperature distribution produces a gentler acceleration and a lower flux; (2) the form of the solution is determined by a unique integration constant. Changes in the coronal conditions could change this constant and render the solution unstable; and (3) the unique supersonic solution is *not* demanded by the equations of the problem. Objections (2) and (3), which are concerned with the form of the solutions, are discussed in Section 3.2.

3.2 The Form of Solutions: Solar Wind Versus Solar Breeze

In 1961 Chamberlain combined an energy equation, namely the first law of thermodynamics, with the equation for heat conduction; this became the third equation of the problem in which the equations of motion and of conductivity were the first and second. The new equation which resulted was

$$\frac{1}{r^2}\frac{d}{dr}\left(\kappa r^2 \frac{dT}{dr}\right) = -kTw\frac{dN}{dr} + \frac{3}{2}Nkw\frac{dT}{dr} \tag{3.20}$$

where most of the symbols are as above and the thermal conductivity is

$$\kappa = \kappa_0\, T^{5/2} \text{ erg/cm-sec-°K} \tag{3.21}$$

re, κ_0 is approximately 5×10^{-7} (c.g.s.). Equation (3.20) states that the rgy flow per second into a volume goes into increasing the volume or into reasing the internal energy. The time derivative is evaluated using

$$\frac{d}{dt} = \frac{\partial}{\partial t} + \mathbf{w} \cdot \nabla \tag{3.22}$$

s equation refers the net energy gain to the mass flow. Equation (3.20) tains the assumption of energy flow into a volume only by conduction; iative losses or mechanical energy deposition are ignored. Thus, unless erwise noted, use of equation (3.20) implies that the coronal heating takes ce only in a thin shell at the base of the corona.

Chamberlain also standardized some of the notation. Besides $\tau = T/T_0$, $\psi = w^2/U^2$, let

$$\lambda(r) = \frac{GM_\odot \mu m_H}{kT_0 r} = \frac{v_{\text{esc}}^2}{U^2} \tag{3.23}$$

re v_{esc} is the escape velocity for protons (see Section 1.2).

quations (3.1) and (3.20) can be written in the new notation, combined, the density eliminated using equation (3.2) to obtain

$$\frac{d}{d\lambda}\left(\frac{\psi}{2} - \lambda + \frac{5}{2}\tau\right) = -\frac{A}{2}\frac{d}{d\lambda}\left(\tau^{5/2}\frac{d\tau}{d\lambda}\right) \tag{3.24}$$

constant A is given by

$$A = \frac{2\kappa_0 r_0 \lambda_0}{kC} = \frac{2\kappa_0 GM_\odot m_H \mu}{k^2 T_0 C} \tag{3.25}$$

ation (3.24) integrates immediately to give

$$\frac{1}{2}\psi - \lambda + \frac{5}{2}\tau = \varepsilon_\infty - \frac{A}{2}\tau^{5/2}\frac{d\tau}{d\lambda} \tag{3.26}$$

left-hand side of this equation contains the kinetic energy, the potential gy, the internal energy ($\frac{3}{2}\tau$), and the potential for adiabatic expansion (τ). s total kinetic and potential energy per particle is equal to the energy at nity (ε_∞) less the energy still to be gained by conduction as the particle es from a given point to an infinite distance.

he disposition of ε_∞ is crucial for determining the physical nature of the . Chamberlain presented arguments for $\varepsilon_\infty = 0$ and numerically integrated solar wind equation to obtain his "solar breeze" models. The param- s of this model near the earth are $w = 18$ km/sec, $T \approx 20{,}000$ °K, and $N_e =$ cm^3.

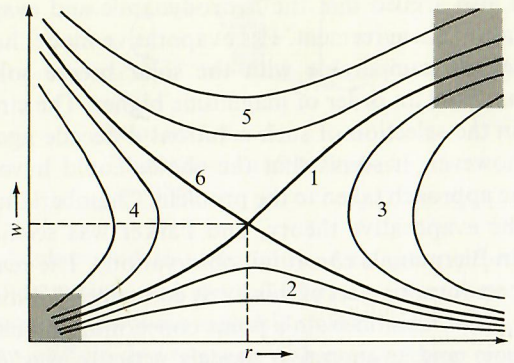

FIGURE 3.3
Different solutions to the "solar wind" equations showing the critical point. (After E. N. Parker.)

Consider again equation (3.7); the basic nature of the solutions is not altered by the introduction of the temperature gradient. The full family of solutions is shown in Figure 3.3. The transonic solar wind solution is curve (1); this curve has $\psi = \tau$ at the critical point. The solar breeze solutions are labeled (2); these curves have $d\psi/d\xi = 0$ at the critical point. Solutions (3) and (4) are double-valued and, hence, unphysical. Solutions (5) and (6) start out supersonic and, therefore, are also unrealistic. Empirical evidence indicates that the solution realized in practice connects the two shaded areas in Figure 3.3. Only the solar wind solutions satisfy this criterion, and it is clear that the solar breeze solutions are not realized in practice.

Nevertheless, the solar breeze curves represent perfectly well-behaved solutions to the wind equations, and they show the property $P \to 0$ as $\lambda \to 0$ ($r \to \infty$). Consideration of the effects of the solar magnetic field on the solar wind (Section 3.7) provides a physical rather than empirical argument for choosing the solar wind or transonic curve.

Chamberlain noted that within the framework of a nonmagnetic corona heated by conduction, equation (3.26) provides an empirical criterion for solar breeze versus solar wind solutions. A solar wind solution requires positive total energy at infinity or $\varepsilon_\infty > 0$. For this to be the case, we must have everywhere $A > 2\lambda/(\tau^{5/2}\, d\tau/d\lambda)$. Thus, if conduction is sufficiently efficient, a solar wind can be attained. Physically, the limit results from the fact that the kinetic energy required for a supersonic solar wind increases with increasing density while conduction (which supplies the energy) is density independent. Thus, for a sufficiently high density, conduction cannot supply enough energy and the supersonic solution cannot be achieved. Noble and Scarf's model (discussed below) satisfied the criterion quoted, but Chamberlain's solar breeze models did not.

Chamberlain also argued that the hydrodynamic and evaporative models hould be in reasonable agreement. His evaporative model had an expansion elocity and density comparable with the solar breeze solution while the mperature was about an order of magnitude higher. The circumstances that ere involved in the selection of such solutions a decade ago were complex; retrospect, however, it seems that the choice could have been adversely fluenced by the approach taken to the problem. Chamberlain was thoroughly miliar with the evaporative theory, and Parker was seeking a theoretical odel to explain Biermann's comet tail observations. The reader is invited to xamine the papers forming part of this lively controversy. Finally, it should be oted in passing that Chamberlain's point concerning the basic similarity of e hydrodynamic and evaporative models actually was correct, but the vaporative model required modification in order to be applicable to the lar corona (see discussion in Section 3.6.).

As noted earlier, the solar wind model first presented by Parker contained undesirable feature: very high fluxes near the earth and very high expansion elocities in the corona. In 1963 Noble and Scarf integrated the solar wind quations given by Chamberlain from the earth inward for the case of small ut finite ε. The parameters adopted at the earth, $N_e = 3.4/\text{cm}^3$, $w = 352$ m/sec, and $T = 2.8 \times 10^5$ °K, are reasonable representations of the observed lar wind, and the computer solution also showed reasonable agreement ith the coronal densities. Thermal conduction alone beyond about $2R_\odot$ is fficient gradually to accelerate the coronal plasma through the critical oint and produce a supersonic expansion at large distances.

Investigators have probed the question of the stability of the solar wind lutions, but the problem is complex and some of the earlier conclusions are ow being questioned. Recently Jockers investigated the stability of an othermal, spherically symmetric solar wind to velocity and pressure pertur- tions which are applied at the inner boundary. He did find stable solutions ut urged further investigation.

Many basic problems are not yet understood, such as the degree to which id behavior is approximated in an essentially collisionless plasma. But one zzling and surprising aspect of the inviscid hydrodynamic models described this section (see also the references) is the fact that they are in better agree- ent with the observations than models with viscosity (see Section 3.4).

3 The De Laval Nozzle Analogy

e process by which the solar corona with typical thermal speeds of 180 n/sec is able to move material against the solar gravitational field (such that e escape velocity is $\approx$ 500 km/sec) and give it a velocity of 400–500 km/sec d beyond may at first sight seem somewhat mysterious, particularly to

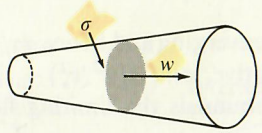

FIGURE 3.4
Quantities related to the flow in tubes.

workers with a background in astronomy. Analagous processes have been known to aerodynamicists and aircraft engineers for some time. Here we explore the physics of supersonic expansion with the help of a nozzle analogy.

Consider a flow of fluid down a tube with cross section σ (Figure 3.4). The equation of continuity becomes

$$\sigma \rho w = \text{const} \tag{3.27}$$

The equation of motion (3.1) neglecting gravity becomes

$$-\rho w\, dw = dP \tag{3.28}$$

where P is the pressure. This equation can be rewritten as

$$\frac{dP}{\rho} = \frac{dP}{d\rho}\frac{d\rho}{\rho} = -w\, dw. \tag{3.29}$$

By specifying the physical nature of the process, we can specify $dP/d\rho$. If the flow is isothermal,

$$\frac{dP}{d\rho} = \frac{v_s^2}{\gamma} \tag{3.30}$$

where v_s is the speed of sound (see equation (3.12)). If the flow is adiabatic,

$$\frac{dP}{d\rho} = v_s^2 \tag{3.31}$$

Here the latter assumption is adopted and equation (3.29) becomes

$$\frac{d\rho}{\rho} = -\frac{w}{v_s^2}\, dw \tag{3.32}$$

Taking logarithms of equation (3.27), differentiating, and evaluating $d\rho/\rho$ from equation (3.32) yields

$$\frac{d\sigma}{\sigma} = \left(\frac{w^2}{v_s^2} - 1\right)\frac{dw}{w} \tag{3.33}$$

This is a fundamental equation. Consider the various possibilities.

Case I: Here the tube is converging and hence $d\sigma/\sigma$ is negative. If the velocity increasing, dw/w is positive, and $[(w^2/v_s^2) - 1]$ must be negative. Thus $< v_s$, and the speed of sound is the limiting flow speed in a converging e.

Case II: Here the cross section of the tube is constant, and $d\sigma/\sigma = 0$. If the ocity is increasing, the relation requires $w = v_s$.

Case III: The tube is diverging and hence $d\sigma$ is positive. If a positive dw/w equired, then $w > v_s$ is indicated.

Thus, a flow can be (1) accelerated to the velocity of sound in a converging e, (2) accelerated through the velocity of sound in a tube of constant cross tion, and (3) accelerated supersonically in a diverging tube. Such a sequence stitutes the basic principle of the de Laval nozzle or rocket engine shown ematically in Figure 3.5. The basic physical process in both the solar wind l the rocket engine is to convert random motions into directed motions. mpare equations (3.7) and (3.33); they are remarkably similar in form. In the ar wind case, solar gravity confines the hot plasma, allows the existence of critical point, and produces the supersonic expansion. In the rocket ine, the chamber walls provide the confinement; the critical point is ated in the throat of the nozzle, and the supersonic expansion results.

The role of gravity and the importance of "confinement" cannot be over-phasized. Consider a subsonic flow in a diverging tube; equation (3.33) tates a negative dw/w, and the velocity of expansion continuously decreases. re there is no throat. Examine once again equations (3.7) to (3.9), and note t the zero in the right-hand side of equation (3.7) depends on the solar vity; if it is too low, the zero does not exist and the solution cannot pass ough the critical point. This fact is the physical origin of the result (pre-ted in Section 3.1) that supersonic expansion cannot occur in a spherical metry for temperatures greater than about 4×10^6 °K. For higher tempera-es, λ [equation (3.5)] is too small, the zero cannot occur, etc. This upper it could be altered by a different geometry, formed for example by magnetic ictures above prominences.

ome theoretical results from the rocket problem may be of interest. The ximum exhaust velocity from a de Laval nozzle is $(3)^{1/2} v_s$; for a 2×10^6 °K ona, the sound speed is 235 km/sec, and the maximum exhaust speed is km/sec. Gravity is not included in this calculation, but the efficiency could greatly increased by heating beyond the throat (where the gas would begin ool adiabatically); this is the principle of the afterburner. If, on the other d, the sound speed is not reached in the throat, the gas decelerates in the erging section. Whether or not this occurs depends on the pressure of the kground medium; the flow into a vacuum is supersonic.

n summary, the solar wind flow, as an important phenomenon with the erved properties noted above, exists only for a limited temperature range. T is too high, there is effectively no throat, and supersonic expansion

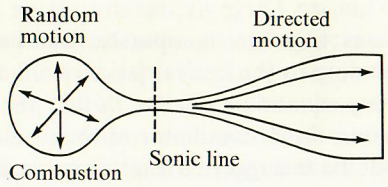

FIGURE 3.5
The de Laval nozzle or rocket engine showing the conversion of random kinetic motions into directed motions.

cannot occur. If T is too low, the situation is essentially static—like a heavy gas in a planetary atmosphere. For the intermediate range with $T \approx 2 \times 10^6$ °K, the supersonic flow occurs in a manner physically similar to the de Laval nozzle in a rocket engine.

3.4 Solutions with Viscosity

The Navier-Stokes equation for a compressible fluid in a steady state is

$$\rho \mathbf{w} \cdot \nabla \mathbf{w} = -\nabla P - \rho \left[\nabla \phi - \frac{w_\phi^2}{r} \mathbf{e}_r \right] \tag{3.34}$$

$$+ \eta^* \nabla^2 \mathbf{w} + (\zeta + \tfrac{1}{3} \eta^*) \nabla (\nabla \cdot \mathbf{w})$$

Here $\phi = -GM_\odot/r$; w_ϕ is the azimuthal velocity; $\mathbf{e}_r$ is a unit radial vector; the viscosity, $\eta^* = 1.2 \times 10^{-16}\, T^{5/2}$ gm/cm-sec; ζ is the second coefficient of viscosity. For an inviscid fluid, spherical symmetry, and $w_\phi = 0$, equation (3.34) reduces to equation (3.1).

The centrifugal force term $\rho(w_\phi^2/r)\mathbf{e}_r$ in equation (3.34) can be roughly estimated by means of an approximation used in studying planetary interiors where the centrifugal force is averaged over a sphere. This averaged force $2\rho w_\phi^2/3r$ is unimportant both for rigid body rotation in the corona and also for realistic values of w_ϕ throughout the solar wind region; this term is included, however, for a model given in Section 3.7.

Studies of the viscous terms in equation (3.34) have been undertaken by several investigators. Normally, the second coefficient of viscosity is set equal to zero. The term $\eta^* \nabla^2 \mathbf{w}$ is the usual viscous term while the term $(1/3)\, \eta^* \nabla (\nabla \cdot \mathbf{w})$ arises from the fact that the gas is compressible ($\nabla \cdot \mathbf{w} = 0$ for an incompressible fluid). Several solar wind models with viscosity have been derived;

they have the common property of giving a very low expansion velocity near the earth of about 165 km/sec. Large viscous stresses are found in these models. These viscous solutions have the computational advantage of having no singularities corresponding to the critical point of the inviscid solution. This can be seen by solving equation (3.7) for $d\psi/d\xi$; the viscous terms (when added) prohibit a zero in the denominator of the resulting expression.

Meyer and Schmidt have suggested that some insight into the physical situation can be obtained through consideration of the viscous stress T. The sum of the viscous terms in equation (3.34) for spherical symmetry can be evaluated from the expression

$$\frac{1}{r^3}\frac{d}{dr}(r^3 T) \tag{3.35}$$

where the usual expression for the viscous stress is

$$T = \frac{4}{3}\eta^*\left[\frac{dw}{dr} - \frac{w}{r}\right] \tag{3.36}$$

The stress is composed of a part resulting from the velocity gradient and a part (w/r) produced by the lateral momentum transfer in a radially diverging flow. The viscous force associated with the lateral momentum transfer has a braking effect and is important even far from the sun.

Meyer and Schmidt have pointed out that the presence of the magnetic field in the solar wind greatly reduces the mean free path perpendicular to the field lines. This reduction, in turn, reduces the lateral momentum transfer. These researches have suggested that the physical situation can be approximated by neglecting the term in (w/r) in equation (3.36) and writing $T = (4/3)\eta^*[dw/dr]$. They have carried this modification through and find a much more reasonable model of the solar wind with an expansion velocity at earth of about 302 km/sec.

These developments show that viscosity should be included in model solar wind calculations, but apparently care must be taken to include the viscosity and the magnetic field and perhaps other effects such as the anisotropic distribution of peculiar velocities in a consistent manner. If the interpretation suggested by Meyer and Schmidt is correct, the viscous solutions with a magnetic field resemble the inviscid solutions. Their interpretation is not universally accepted however, and the authors themselves have noted that it is probably in error. If it is incorrect, some other explanation will be needed for the serious discrepancy between the viscous solutions and the inviscid solutions, which show good agreement with the observations. The situation involves the concept and calculation of viscosity in a dilute gas which does not experience ordinary collisions.

3.5 Two-Fluid Models

The solar wind models described in the preceding sections of this chapter have all been, in effect, one-fluid models. The fluid was ideally composed solely of particles with mass $\mu\, m_H$, all of which can be adequately described at each point by one density, one velocity, and one temperature. This basic concept is not vitiated by evaluating the conductive heat transport with the correct expression for a proton-electron gas.

Sturrock and Hartle have pointed out that the single-fluid models contain an implicit and probably indefensible assumption concerning the rate of energy exchange between the protons and electrons. In particular, the protons and electrons could have substantially different temperatures far from the sun.

Some physical insight into the temperature inequality can be obtained by considering the expansion rate versus the energy exchange rate. The expansion rate is

$$v_{\exp} = \frac{w}{N_e}\frac{dN_e}{dr} \tag{3.37}$$

This can be approximated away from the sun where $N_e \propto r^{-2}$ by

$$v_{\exp} \approx \frac{2w}{r} \tag{3.38}$$

Near the earth, we take $w = 500$ km/sec to obtain $v_{\exp} \approx 6 \times 10^{-6}$ sec^{-1}. The energy exchange rate is available from standard expressions of plasma physics and is

$$v_E \approx 1 \times 10^{-1}\frac{N_e}{T_e^{3/2}} \tag{3.39}$$

Near the earth, we take $N_e = 5/\text{cm}^3$ and find $v \approx 5 \times 10^{-7}$ sec^{-1} for $T_e = 10^4$ °K. Clearly, T_e would have to be $\sim 10^3$ °K for equality of v_E and $v_{\exp}$. For $v_E \gg v_{\exp}$, a T_e much less than 10^3 °K would be required. These are orders of magnitude less than the anticipated and measured values of T_e throughout the interplanetary medium, and considerable differences between T_e and T_p would, therefore, be expected.

Hartle and Sturrock have investigated a two-fluid model of the solar wind. Only the temperatures of the two fluids can be significantly different. Both densities and flow velocities must be the same to preserve local charge neutrality and to keep the sun electrically neutral, respectively. (Recall the discussion in Section 1.2). Hence we have one equation of continuity (3.2) and one equation of motion,

$$N_e m_H w\frac{dw}{dr} = -\frac{d}{dr}[N_e k(T_e + T_p)] - \frac{GM_\odot m_H N_e}{r^2} \tag{3.40}$$

originate entirely in the corona; (2) the He^+ originates by charge-exchange of He^{++} with neutral hydrogen in the interplanetary medium; or (3) the He^+ originates by charge-exchange of He^{++} with terrestrial neutral hydrogen in an extended cloud around the earth. This latter possibility must be considered because the Vela probes are in a nearly circular orbit with a radius of about 17 R_E. The first possibility appears unlikely because the ratio O^{+7}/O^{+6} is entirely consistent with the solar wind originating in the corona. It is difficult to favor either the second or third hypothesis. The second would imply far more neutral hydrogen (presumably of interstellar origin) in the interplanetary medium than expected from our discussion in Section 3.10. The third would appear to require a more extended and denser terrestrial hydrogen cloud than is currently considered plausible. Direct observation of neutral hydrogen atoms in the solar wind or the interplanetary medium should resolve this problem.

5.5 The Magnetic Field

The interplanetary magnetic field is an integral part of the solar wind and is the photospheric field extended outward by the expansion of the plasma. From the theory presented in Sections 3.1 and 3.7, we would expect an average field near earth of about 5γ; the solar rotation leads to the development of the characteristic Archimedean spiral with an angle of about 45°. Available observations confirm this general picture.

A histogram (based on observations covering three solar rotations; see Figure 5.10) shows the distribution of field magnitude that was obtained by Ness, Scearce, and Cantarano from IMP-1 data. The median value is 5.5γ

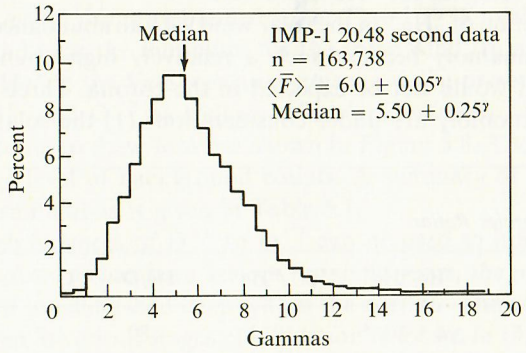

FIGURE 5.10
The distribution of interplanetary magnetic field magnitude as observed by IMP-1 from 1963 to 1964. (Courtesy N. F. Ness.)

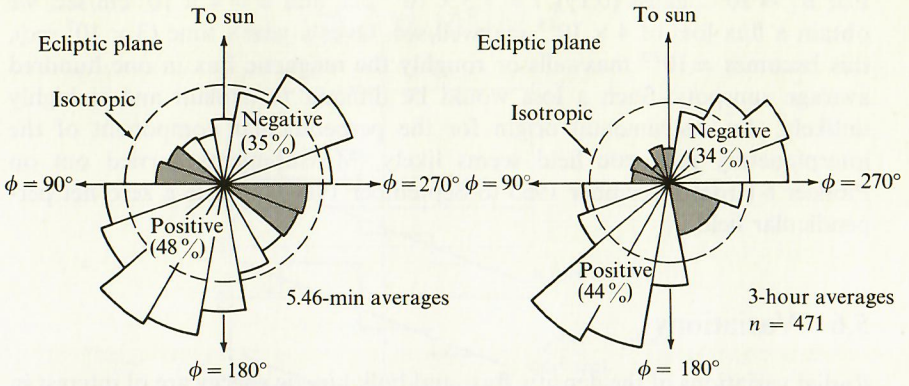

FIGURE 5.11
The distribution of interplanetary field directions observed by IMP-1; note the change when a longer averaging period is used. (Courtesy N. F. Ness, C. S. Scearce, J. B. Seek, and J. M. Wilcox.)

($1\gamma = 10^{-5}$ gauss). Extreme values of the field magnitude are a low of about 0.25γ and a high near 40γ. Vector magnetic fields can currently be measured to within $\pm 0.25\gamma$; such an accuracy is dependent on the construction of nonmagnetic spacecraft.

The directional properties of the magnetic field are determined by plotting histograms of field direction as projected into the plane of the ecliptic (see Figure 5.11); the 7° difference between the plane of the solar equator and the plane of the ecliptic is unimportant for this discussion. The clear tendency of the field to lie along angles in a solar-ecliptic coordinate system of 135° or 315° (corresponding to a spiral angle of 45°) is shown, particularly when the results are averaged over a longer time period. Hence, a gross overall Archimedean spiral geometry is indicated, but with a substantial amount of local irregularity.

Measurements made on board Mariner 2, Pioneer 5, and IMP-1 have indicated a southward component of field perpendicular to the plane of the ecliptic amounting to about 1γ. If such a permanent component persists across a sector boundary (see Section 5.6) where the field changes direction (say) from toward to away from the sun, the angle that the field lines make with the ecliptic plane must change sign; Dessler has pointed out the disagreeable nature of this possibility. Davis has warned of the severe consequences of such a component for the solar magnetic field. If the magnetic flux is frozen-in, the time rate of change of a net magnetic flux through the plane of the ecliptic is

$$\frac{\partial \Phi}{\partial t} = 2\pi r w B_\perp \tag{5.3}$$

For $B_\perp = 10^{-6}$ gauss (0.1γ), $r = 1.5 \times 10^{13}$ cm, and $w = 4 \times 10^7$ cm/sec, we obtain a flux loss of 4×10^{15} maxwell/sec. Over a year's time (3×10^7 sec), this becomes $\approx 10^{23}$ maxwells or roughly the magnetic flux in one hundred average sunspots. Such a loss would be difficult to explain and is highly unlikely. An instrumental origin for the perpendicular component of the interplanetary magnetic field seems likely. Measurements carried out on Pioneer 6 (from December 1965 to September 1966) indicate a zero net perpendicular field.

5.6 Variations

Radial variations of the density, flux, and bulk kinetic energy are of interest in themselves as well as providing checks on our theoretical understanding. Neugebauer and Snyder have compared these quantities observed on Mariner with the expected inverse square variation (Figure 5.12), and the theoretical expectation is verified. The radial variation of the total magnetic field was studied on Pioneer 6 for 0.81 a.u. $< r <$ 1.0 a.u. by Burlaga and Ness and on Mariner 4 for 1.0 a.u. $< r <$ 1.5 a.u. by Coleman, Smith, Davis, and Jones. The field strength for the latter experiment could be approximated by $B = 4.13\ (r/r_0)^{-1.25}$ where $r_0 = 1.5$ a.u. and the field is in γ; an ideal spiral field in a quiet solar wind at 350 km/sec would have $B \propto (r/r_0)^{-1.29}$.

Variations in the density and solar wind velocity during the flight of Mariner 2 have been presented by Neugebauer and Snyder, and these are shown in Figure 5.13. These data clearly show that high velocity is correlated with low density, and vice versa. Thus, the flux wN_e tends to be somewhat constant. Vela measurements show that high proton temperatures are observed when the bulk velocity is high and that low temperatures are observed when the velocity is low. Eventually, acceptable models of the solar wind will have to explain these gross features. Variations of w with geomagnetic index Kp are also known, but we defer this discussion until consideration of the "sector structure" (below).

A great deal of information is available about the variations in the magnetic field. Ness has pointed out that we have

$$\left[\frac{dB_I}{dt}\right]_{\text{observed}} = \frac{\partial B_I}{\partial t} + (\mathbf{w} \cdot \nabla)B_I \tag{5.4}$$

where B_I is the interplanetary field. Since the solar wind speed is some five to ten times any magnetohydrodynamic wave speed, the second term in equation (5.4) dominates. Thus, the major observed change is due to convection of different regions past the observer. With this fundamental limitation in mind, consider the interpretation of variations in (say) the magnetic field

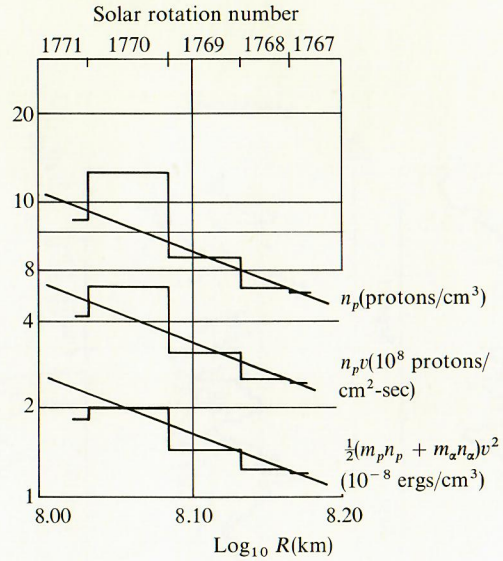

FIGURE 5.12

The radial variation of density, momentum, and energy averaged over a solar rotation obtained from Mariner 2. (Courtesy M. Neugebauer and C. W. Snyder, and the *Journal of Geophysical Research*.)

observed as a function of time. Should these variations be interpreted as waves or discontinuities or whatever? Coleman has searched for the "signatures" of different wave forms and has reported evidence for Alfvén and/or fast mode waves. Sari and Ness have proposed a rather different interpretation. Analyses of time variations of the interplanetary magnetic field are often carried out in terms of "power spectra" which are the square of the Fourier transform of the observed variation. Sari and Ness note that individual discontinuities (and a random distribution of discontinuities) have a power spectrum proportional to $(\textit{frequency})^{-2}$ and that such a dependence is evident in data obtained from Pioneer 6 for the appropriate frequency range (2.8×10^{-4} to 1.6×10^{-2} c/s) and well above the noise level. This behavior is attributed to directional discontinuities in the microstructure (see below for definition), and such discontinuities alone are sufficient to explain the power spectra. At lower frequencies, the interplanetary macrostructure shows up in the power spectra. The overall situation is not yet entirely settled. A sample of data showing some discontinuities in the solar wind is given in Figure 5.14.

Burlaga and Ness have suggested three scales of observing time in which to classify interplanetary phenomena: (1) microstructure, $t \leq 1$ hours; (2)

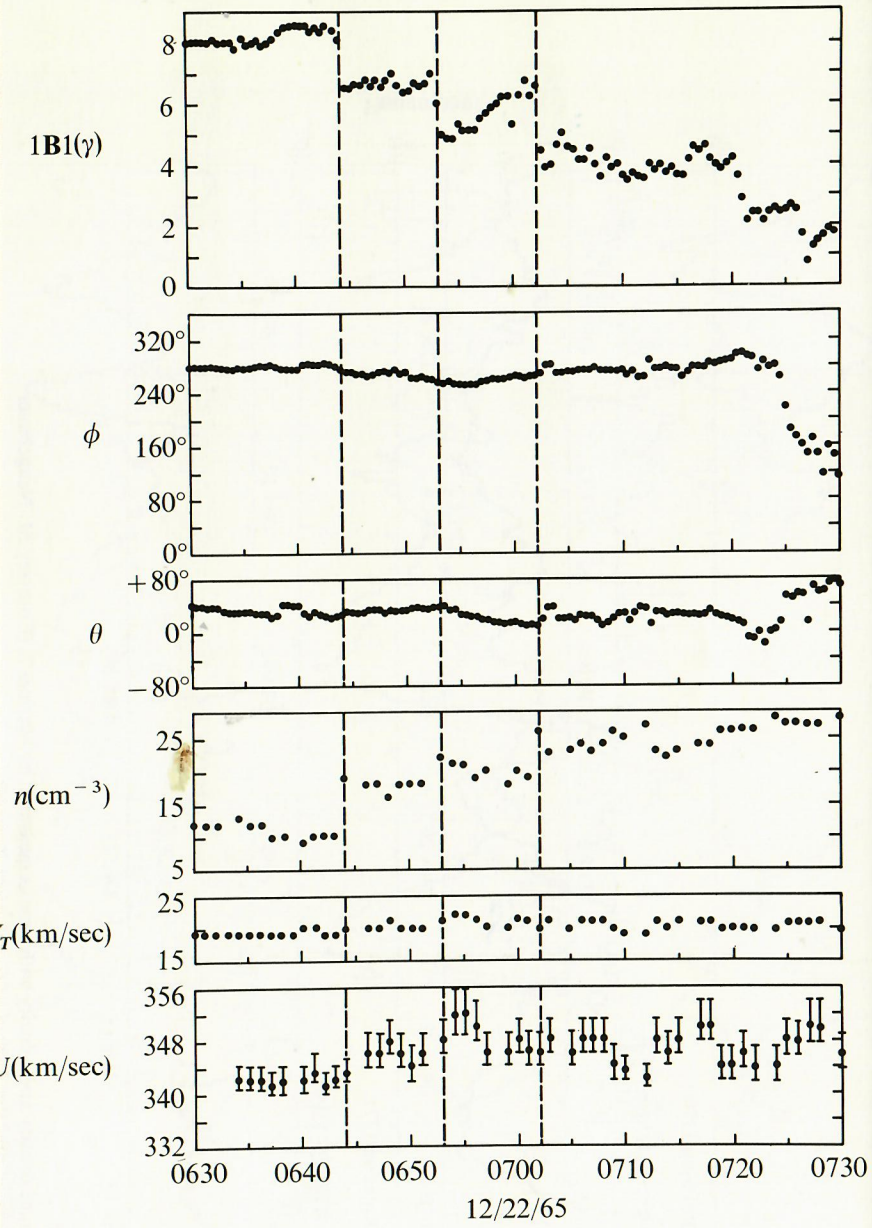

IGURE 5.14

Sample data showing discontinuities in the solar wind; U is the bulk velocity, V_T is the thermal velocity, ϕ is the azimuthal angle shown in Figure 5.11, and θ is the polar angle ($\theta=0$ in the ecliptic); ϕ and θ refer to the direction of B. (Courtesy L. F. Burlaga.)

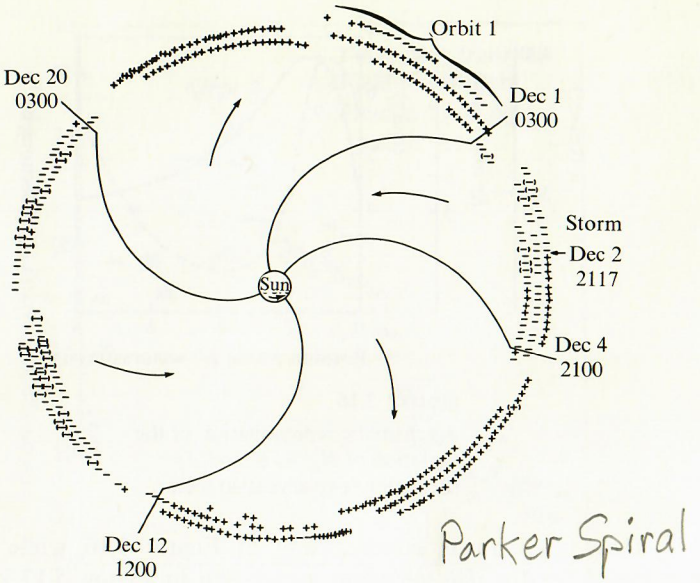

FIGURE 5.15

The sector structure of the interplanetary magnetic field observed by IMP-1. The plus or minus polarities correspond to the positive and negative directions indicated in Figure 5.11. Polarities in parentheses correspond to a movement into the shaded area of Figure 5.11 for a few hours in a smooth and continuous manner. (Courtesy N. F. Ness and J. M. Wilcox.)

mesostructure, $1h \leq t \leq 10^2$ hours; and (3) macrostructure, $t > 10^2$ hours. These observing times scale naturally into length scales by multiplying them by an average solar wind velocity of about 400 km/sec. Then, we find: (1) microstructure, $l(\mu s) < 10^6$ km ≈ 0.01 a.u.; (2) mesostructure, l(meso) $\sim 10^6$–10^8 km ~ 0.01–1.0 a.u.; and (3) macrostructure, l(macro) $> 10^8$ km ≈ 1 a.u.

The microstructure corresponds to shock waves and the contact discontinuities; these features can act as scattering centers for cosmic rays. The mesostructure corresponds to filaments or kinks in the field structure. These are the "flux tubes" responsible for channeling of cosmic rays (Section 6.7). The ultimate origin of this scale of structure may be in the solar supergranulation described in Section 2.2.

Finally, the macrostructure manifests itself as a longitudinal variation in the magnetic field first discovered by Ness and Wilcox which they called the "sector structure." Individual sectors contain a magnetic field of constant polarity as shown in Figure 5.15. The sector boundaries are sharp ($< 10^5$ km) and relatively stable in time. Changes do occur, however. Regular variations of magnetic field magnitude, w, Kp, and N_e are found in the individual